

Med-R1: Reinforcement Learning for Generalizable Medical Reasoning in Vision-Language Models

Yuxiang Lai, Jike Zhong, Ming Li, Shitian Zhao, Yuheng Li, Konstantinos Psounis, *Fellow, IEEE*, and Xiaofeng Yang, *Member, IEEE*

arXiv:2503.13939v5 [cs.CV] 27 Oct 2025

Abstract— Vision-language models (VLMs) have achieved impressive progress in natural image reasoning, yet their potential in medical imaging remains underexplored. Medical vision-language tasks demand precise understanding and clinically coherent answers, which are difficult to achieve due to complexity of medical data and the scarcity of high-quality expert annotations. These challenges limit the effectiveness of conventional supervised fine-tuning (SFT) and Chain-of-Thought (CoT) strategies that work well in general domains. To address these challenges, we propose Med-R1, a reinforcement learning (RL)-enhanced VLM designed to improve generalization and reliability in medical reasoning. Med-R1 adopts Group Relative Policy Optimization (GRPO) to encourage reward-guided learning beyond static annotations. We comprehensively evaluate Med-R1 across *eight* distinct medical imaging modalities. Med-R1 achieves a 29.94% improvement in average accuracy over its base model Qwen2-VL-2B, and even outperforms Qwen2-VL-72B—a model with $36\times$ more parameters. To assess cross-task generalization, we further evaluate Med-R1 on *five* question types. Med-R1 outperforms Qwen2-VL-2B by 32.06% in question-type generalization, also surpassing Qwen2-VL-72B. We further explore the thinking process in Med-R1, a crucial component of Deepseek-R1. Our results show that omitting intermediate rationales (*No-Thinking Med-R1*) not only improves cross-domain generalization with less training, but also challenges the common assumption that more reasoning always helps. Nevertheless, we also find that the *Think-After Med-R1* variant further improves performance while maintaining interpretability. These findings suggest that in medical VQA, it is not the presence of reasoning itself, but rather its *quality and position*. Together, these results highlight that RL improves medical reasoning

Equal contribution: Yuxiang Lai, Jike Zhong, and Ming Li. Corresponding author: Xiaofeng Yang (email: xiaofeng.yang@emory.edu).

This work is supported in part by the National Institutes of Health under award numbers R01CA272991, R01EB032680, R01DE033512, and U54CA274513.

Yuxiang Lai and Xiaofeng Yang are with the Department of Computer Science and Informatics, Emory University, Atlanta, GA 30322, USA.

Jike Zhong and Konstantinos Psounis are with Department of Computer Science and Department of Electrical and Computer Engineering, University of Southern California, Los Angeles, CA 90089, USA.

Ming Li is with the Department of Computer Science, University of Tokyo, Tokyo 113-8654, Japan.

Shitian Zhao is with the Department of Computer Science, Johns Hopkins University, Baltimore, MD 21218, USA.

Yuheng Li and Xiaofeng Yang are with the Department of Biomedical Engineering, Georgia Institute of Technology and Emory University, Atlanta, GA 30332, USA. Xiaofeng Yang is also with the Department of Radiation Oncology and Winship Cancer Institute, Emory University, Atlanta, GA 30322, USA.

and generalization, enabling efficient and reliable VLMs.

Index Terms— Reinforcement Learning, Vision Language Models, Multimodal LLM, Post-Training, Medical Reasoning.

I. INTRODUCTION

VISION-LANGUAGE MODELS (VLMs) have achieved strong performance on natural image understanding tasks such as visual question answering (VQA) and multimodal dialogue [1]–[3], enabled by large-scale pretraining and supervised fine-tuning (SFT). However, applying VLMs to medical imaging remains challenging due to the need for clinically sound interpretations and decision-making processes. Medical tasks often involve multi-step analysis—e.g., diagnosing a lung nodule may require integrating lesion localization, morphology, and context. In addition, the diversity of imaging modalities (e.g., CT, MRI) and task types (e.g., diagnosis, grading) imposes demands on generalizability. This raises a key question: how can we enable VLMs to perform well across medical domains while ensuring reliable and context-aware behavior?

In this paper, we identify that the limitations of current medical VLMs primarily stem from the inherent drawbacks of Supervised Fine-Tuning (SFT) [4], [5]. While SFT has been widely adopted to adapt foundation models to medical imaging [6]–[10], it suffers from two fundamental issues that hinder medical applicability. First, SFT inherently biases models toward memorizing task-specific shortcuts rather than learning generalizable reasoning. By directly aligning model outputs with final answers (e.g., diagnostic labels), SFT encourages overfitting to superficial patterns in training data. Second, the scarcity of high-quality Chain-of-Thought (CoT) annotations severely limits the effectiveness of SFT in medical reasoning. Unlike general-domain tasks, where large-scale CoT datasets can be crowdsourced, medical reasoning requires domain-specific logical structuring (e.g., systematically ruling out differential diagnoses before confirming malignancy). However, curating such CoT datasets is prohibitively expensive, as it demands meticulous annotation by experienced medical professionals to ensure diagnostic validity and clinical coherence. As a result, existing SFT-based medical VLMs [6], [7] lack access to high-quality CoT data, leading to shallow reasoning with limited clinical rigor. These models frequently produce "black-box" predictions, struggling to provide traceable reasoning

or maintain performance in out-of-domain tasks. This lack of transparency and robustness poses a significant challenge to medical adoption, where explainability and reliability are indispensable requirements.

To address these challenges, we propose Med-R1, a reinforcement learning (RL)-based framework for enhancing the generalizability and interpretability of medical VLMs. Unlike SFT, which aligns outputs to fixed supervision and often leads to shortcut learning, RL encourages exploration of diverse reasoning strategies through reward signals—without requiring explicit CoT annotations [11]. We adopt Group Relative Policy Optimization (GRPO) [12], a lightweight alternative to PPO (Proximal Policy Optimization) [13] that stabilizes training via rule-based rewards and group-relative comparisons. These mechanisms reduce computational overhead while encouraging clinically grounded reasoning, making GRPO well-suited for medical tasks where scalability and reliability are essential.

As shown in Figure 1, we evaluate Med-R1 across eight diverse medical imaging modalities, including CT, MRI, Ultrasound, Dermoscopy, Fundus Photography, OCT, Microscopy, and X-ray. These modalities cover a wide range of clinical imaging—from macroscopic anatomy to cellular-level and functional assessments. Med-R1 (2B parameters) achieves 69.91% average accuracy, a 29.94% gain over its base model Qwen2-VL-2B, and even outperforms the 72B-parameter Qwen2-VL-72B (Table IV), highlighting the benefit of RL-driven adaptation. We further assess generalizability across five question types: modality recognition, anatomy identification, disease diagnosis, lesion grading, and biological attribute analysis. Med-R1 improves question-type generalization accuracy by 32.06% over Qwen2-VL-2B and surpasses Qwen2-VL-72B in this setting as well (Table VIII). These demonstrate that RL enhances both parameter efficiency and generalizability in medical VLMs.

Finally, we investigate the impact of intermediate rationales in Med-R1. Conventional wisdom suggests that explicit step-by-step reasoning (“Think”) enhances generalization, yet our results show this is not always true in medical VQA. We compare three RL post-training strategies: (1) *Think*, which generates rationales before answering; (2) *No-Think*, which directly predicts the answer; and (3) our proposed *Think After*, which performs concise reasoning *after* prediction. We find that *No-Think* improves generalization across modalities, while *Think* often causes hallucinated rationales due to domain shift. In contrast, *Think After* preserves interpretability without sacrificing accuracy, striking the best balance between reliability and explainability. These findings reveal that in specialized domains, the effectiveness of reasoning depends more on its quality, timing, and domain alignment than its length, challenging the notion that “more thinking is better.”

Med-R1 a comprehensive and systematic study of rule-based RL for medical reasoning across eight imaging modalities (Figure 2). We summarized our contribution as follows:

1) Multi-modality and multi-task medical reasoning

VLM. We propose *Med-R1*, a comprehensive and systematic study of rule-based reinforcement learning for medical reasoning, supporting **eight imaging modalities** (CT, MRI, Ultrasound, etc.) across **five distinct clinical tasks**. We demonstrate that RL-based fine-tuning

effectively promotes modality-specific as well as cross-modality reasoning in the medical domain without the need for token-level supervision as in SFT. The proposed Med-R1 is capable of generating step-by-step, accurate, and plausible explanations.

- 2) **Robust Generalization with Efficiency.** We show that alongside the solid modality and task-specific performance, Med-R1 exhibits strong **generalization**. Med-R1 outperforms the base model by **29.94%** and SFT baselines by **15.84%** in average generalization accuracy across modalities. In cross-task settings, it outperforms the base model and SFT baseline by **32.06%** and **11.25%** respectively. Moreover, Med-R1 surpasses other larger generic or medical-specific models including Qwen2-VL-72B, and MedViNT-7B, warranting its efficiency and reliability for real-world deployment.
- 3) **Rethinking the “More Thinking is Better” Assumption:** Our results challenge the common belief that generating longer or more explicit reasoning chains necessarily improves generalization. We find that reinforcement learning without explicit reasoning often yields higher accuracy, as free-form reasoning learned from general-domain data can induce hallucinations under domain shift. However, this may reduce reliability and interpretability in medical applications. To address this, we introduce *Think-After*—a reasoning scheme where the model provides rationalization for its chosen answer *after* the prediction. This design preserves interpretability while mitigating the instability introduced by lengthy reasoning chains, offering a balance between accuracy and explainability. Our findings suggest that the *quality* and *timing* of reasoning are critical for robust generalization.

II. RELATED WORKS

General VLMs and Medical VLMs. General-purpose VLMs such as CLIP [14] and BLIP-2 [15] have advanced natural image-text understanding via large-scale pretraining, but struggle with domain-specific tasks like medical reasoning. Recent efforts adapt VLMs through supervised fine-tuning (SFT) on medical datasets, as seen in LLaVA-Med [8] and Med-Flamingo [6]. While effective in-domain, these models often overfit to narrow corpora and lack generalization across modalities or task types. Our work addresses this limitation by introducing RL for scalable, modality-agnostic adaptation.

Reinforcement Learning for Post-Training. RL has shown promise for aligning language models with desired behavior via reward feedback [16], [17]. In vision-language tasks, RL improves VQA accuracy [11] and reduces hallucination [12], but often relies on complex reward models or costly human supervision. GRPO [12] offers a scalable alternative by using rule-based rewards and group-relative comparisons. We extend this approach to medical VQA, enabling efficient adaptation without modality-specific supervision.

Medical Reasoning and Interpretability Interpretable reasoning is critical in medical AI, with recent work exploring CoT prompting [18] and program-guided logic [4]. However, such methods rely on costly expert annotations [19], limiting

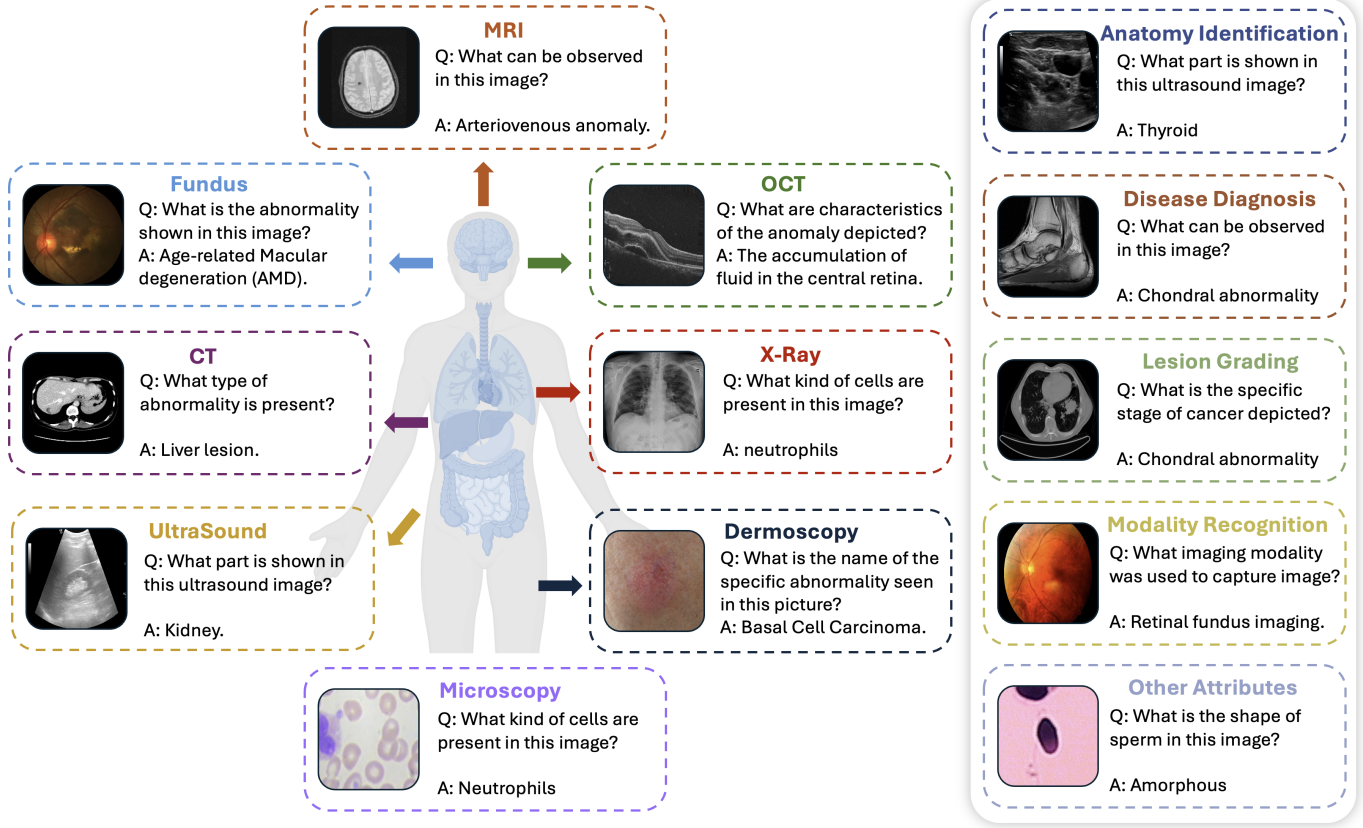


Fig. 1. Overview of the Evaluation Framework: Eight Medical Imaging Modalities and Five Medical Vision Question Answering Tasks. We evaluate Med-R1 across eight distinct medical imaging modalities—Computed Tomography (CT), Magnetic Resonance Imaging (MRI), Ultrasound, Dermoscopy, Fundus Photography, OCT (Optical coherence tomography), Microscopy Images, and X-ray Imaging—as well as five medical vision question answering tasks: anatomy identification, disease diagnosis, lesion grading, modality recognition, and biological attribute analysis. Example images and corresponding clinical questions illustrate the diversity of medical data and the challenges in developing generalizable vision-language models for automated medical reasoning.

scalability in clinical domains. Reinforcement learning offers an alternative by enabling emergent reasoning without explicit supervision. Concurrently, MedVLM-R1 [20] also applies GRPO-based RL to radiology VQA, which is focuses on a single radiology-specific setting (training on MRI and testing on CT and X-ray) and reports generalization within radiology, using roughly 600 training samples. Nonetheless, it highlights the growing interest in RL for medical VLMs.

III. METHOD

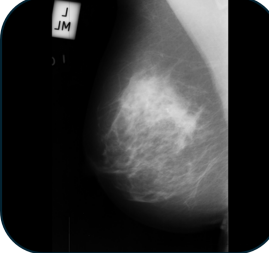
We adopt rule-based RL to encourage multimodal reasoning and generalization in medical domains. Recent studies have demonstrated that RL can incentivize emergent logical reasoning and generalization in multimodal tasks such as mathematical reasoning [21] and visual navigation [11]. Building on these insights, we extend its application to the medical domain and systematically assess its effectiveness in this context. Specifically, we leverage the popular RL-based post-training method GRPO [22] to train a large base MLLM [23] across 8 different modalities for medical reasoning and compare it with zero-shot and SFT performance of popular existing VLMs. We introduce the details of the SFT and RL algorithm, our reward design, and data structure below.

Supervised Fine-tuning: We performed supervised fine-tuning

(SFT) on the Qwen2-VL-2B and Qwen2.5-VL-3 models. Specifically, we fine-tuned the model using mixed-precision training (bfloat16) with gradient accumulation and checkpointing enabled for memory efficiency. The maximum sequence length was set to 4096 tokens, allowing the model to process full visual-text reasoning sequences. Training was conducted for one epoch with a learning rate of 2×10^{-5} , cosine learning-rate scheduling, and a warm-up ratio of 0.1. The per-device batch size was 4, and the gradient accumulation step was 16, resulting in an effective batch size of 64.

A. Group Relative Policy Optimization (GRPO)

Overview: RL-based algorithms such as PPO [13] and GRPO [12] belong to a family of fine-tuning and alignment strategies explicitly designed to enhance models' reasoning capacities. Unlike supervised fine-tuning, which directly optimizes maximum likelihood, these RL-based methods instead optimize the policy gradient using reward signals, encouraging reasoning by exploring a much larger solution space. GRPO is closely related to PPO but differs in two key aspects: first, GRPO estimates the advantage using group-based estimation rather than a value function; second, it employs a set of fixed rules as the reward signal instead of a learned reward model. These optimizations



Problem: What does this image depict in terms of its content?

A) Brain tissue
B) Intestinal tissue
C) Kidney tissue
D) Breast tissue

Med-R1 Response:

Think: The image appears to be a mammogram, which is a type of X-ray used to detect abnormalities in the breast tissue. The presence of dense, irregular patterns and a central area of lighter density suggest the presence of breast tissue.

Answer: D

Groundtruth: D



Problem: What is the specific abnormality present in this image?

A) Pneumonia
B) Sinusitis
C) Urolithiasis
D) Osteoporosis

Med-R1 Response:

Think: The image is a computed tomography (CT) scan of the abdomen, which is a medical imaging technique used to visualize internal structures. The specific abnormality present in this image is not immediately clear from the visible structures alone. However, the presence of a large, dense mass in the right lower quadrant of the abdomen could suggest a urolithiasis.

Answer: C

Groundtruth: C

Fig. 2. Medical VQA examples of Med-R1 The left panel shows a modality recognition task, where the model correctly identifies the presence of breast tissue in a mammogram (X-ray). The right panel illustrates a disease diagnosis task, where Med-R1 accurately detects urolithiasis in an abdominal CT scan. In both cases, the model provides reasoning (“Think”), explaining its decision-making process before selecting the final answer.

make GRPO 50% more resource- and computation-efficient than PPO [12].

Definition: Formally, let $P(Q)$ denote the question set used for training, where q is a sampled question in the current iteration. Let $\pi_{\theta_{\text{old}}}$ and $\pi_{\theta_{\text{new}}}$ denote the old policy and current (new) policy, respectively, where o is a complete response sampled from a policy. Let $\pi_{\theta_{\text{ref}}}$ denote the reference policy, which in practice is the frozen base MLLM. Let G be the number of responses sampled per question in each iteration. The GRPO objective is given by:

$$\begin{aligned} \mathcal{J}_{\text{GRPO}}(\theta) = & \mathbb{E}_{q \sim P(Q), \{o_i\}_{i=1}^G \sim \pi_{\theta_{\text{old}}}(O|q)} \\ & \frac{1}{G} \sum_{i=1}^G \left[\min \left(\frac{\pi_{\theta_{\text{new}}}(o_i | q)}{\pi_{\theta_{\text{old}}}(o_i | q)} \right) A_i, \right. \\ & \left. \text{clip} \left(\frac{\pi_{\theta_{\text{new}}}(o_i | q)}{\pi_{\theta_{\text{old}}}(o_i | q)}, 1 - \epsilon, 1 + \epsilon \right) A_i \right) \\ & - \beta \mathbb{D}_{\text{KL}} \left(\pi_{\theta_{\text{new}}} \parallel \pi_{\theta_{\text{ref}}} \right) \end{aligned} \quad (1)$$

where $\frac{\pi_{\theta}(o_i | q)}{\pi_{\theta_{\text{old}}}(o_i | q)}$ is the policy ratio, and A_i is the estimated advantage, and ϵ is the clipping threshold for policy updates. The KL divergence term [24] regularizes the policy update, ensuring that π_{θ} does not deviate excessively from the reference model $\pi_{\theta_{\text{ref}}}$. Unlike PPO, which uses a critic model to estimate the advantage A_i for a single response o , GRPO estimates the relative advantage by sampling a group of responses $\{o_i\}_{i=1}^G$ and normalizing their rewards within the group to compute a relative advantage [12], [25]. Each reward is calculated based on rules without reward models. We detail reward design below.

Reward design: We follow [12] and use two types of reward:

format and accuracy. Firstly, we prompt the model to explicitly output its thinking process in the “<think>...</think>” tag and the final answer in the “<answer>...</answer>” tag. The format reward is designed to check if the aforementioned tags are present in the final response. A reward score of 1 will be given if they exist and are correct. This helps the model to organize its thoughts and answer in a structured format for the ease of reading. The accuracy reward is a rule-based reward that checks if the actual answer matches with the ground truth. Similarly, a reward score of 1 is given when the results match. In practice, the ground truths are letter options “A, B, C, D” for multiple choice questions, and we treat all responses with correct letter options as the leading word as correct (“A...”).

B. No-Thinking Med-R1

Previous work [26] found that, in image classification tasks, removing both reasoning and format supervision during RL could sometimes improve performance. However, that finding is specific to structured classification tasks with simple output space, where reasoning is rarely required. In contrast, medical VQA involves multimodal, semantically complex inputs, and reasoning failures can arise from domain mismatch rather than verbosity alone [6], [12]. Given the difficulty of obtaining reliable CoT annotations in medical settings, we further investigate the role of intermediate reasoning in RL post-training. We revise the instruction prompt as {Question}. Output the single-letter choice (A, B, C, D, ...) in <answer>...</answer> tags., where {Question} will be replaced by each specific question. By doing so, we encourage the model only to output the final answer without any explicit thinking process. The accuracy reward is maintained, where the reward score is 1 when the

TABLE I

CROSS-MODALITY GENERALIZATION PERFORMANCE OF MED-R1 WITH RL POST-TRAINING. ACCURACY (%) ACROSS EIGHT MEDICAL IMAGING MODALITIES, WHERE ROWS INDICATE TRAINING MODALITIES AND COLUMNS TEST MODALITIES. DARKER CELL SHADES INDICATE HIGHER ACCURACY FOR CORRESPONDING TRAINING-TEST PAIRS IN EACH COLUMN. THE BASE MODEL IS QWEN2.5-VL-3B.

RL fine-tuned Qwen2.5-VL-3B									
Test Train	CT	MRI	X-Ray	Ultrasound	Dermoscopy	Fundus	OCT	Microscopy	Overall
CT	94.35 ± 0.79	70.85 ± 1.10	86.50 ± 1.70	35.44 ± 2.05	66.77 ± 2.53	76.41 ± 2.51	84.08 ± 2.48	66.58 ± 2.79	72.62 ± 0.65
MRI	72.79 ± 1.53	98.57 ± 0.29	83.72 ± 1.80	38.38 ± 2.07	68.30 ± 2.53	79.78 ± 2.32	85.97 ± 2.36	67.12 ± 2.79	74.33 ± 0.64
X-Ray	78.90 ± 1.39	59.73 ± 1.20	93.50 ± 1.21	38.28 ± 2.10	65.85 ± 2.57	76.05 ± 2.55	78.89 ± 2.77	65.14 ± 2.79	69.54 ± 0.68
Ultrasound	62.20 ± 1.67	63.00 ± 1.19	79.57 ± 1.98	98.84 ± 0.46	64.09 ± 2.57	72.22 ± 2.60	78.54 ± 2.77	69.82 ± 2.75	73.53 ± 0.65
Dermoscopy	64.30 ± 1.65	60.39 ± 1.18	80.56 ± 1.92	40.21 ± 2.12	84.99 ± 1.91	71.86 ± 2.69	74.76 ± 2.89	65.23 ± 2.75	67.79 ± 0.70
Fundus	68.59 ± 1.59	61.32 ± 1.19	81.98 ± 1.86	37.42 ± 2.10	67.84 ± 2.49	90.62 ± 1.68	79.13 ± 2.71	66.76 ± 2.79	69.21 ± 0.67
OCT	81.06 ± 1.34	73.92 ± 1.06	83.65 ± 1.80	35.78 ± 2.03	68.99 ± 2.53	80.87 ± 2.32	98.70 ± 0.77	67.12 ± 2.79	73.76 ± 0.65
Microscopy	65.50 ± 1.62	62.34 ± 1.21	80.31 ± 1.95	37.37 ± 2.10	64.24 ± 2.60	71.40 ± 2.64	77.36 ± 2.83	88.02 ± 1.94	68.32 ± 0.69
Overall	73.46 ± 1.51	68.77 ± 1.12	83.72 ± 1.79	45.21 ± 2.14	68.88 ± 2.45	77.40 ± 2.50	82.18 ± 2.53	69.47 ± 2.74	71.14 ± 0.67

CT - Computed Tomography; MRI - Magnetic Resonance Imaging; US - Ultrasound; Der - Dermoscopy; FP - Fundus Photography.

OCT - Optical Coherence Tomography; Micro - Microscopy Images; X-Ray - X-Ray Imaging

TABLE II

CROSS-MODALITY GENERALIZATION PERFORMANCE OF MED-R1 WITH NO-THINK RL POST-TRAINING. ACCURACY (%) ACROSS EIGHT MEDICAL IMAGING MODALITIES, WHERE ROWS INDICATE TRAINING MODALITIES AND COLUMNS TEST MODALITIES. DARKER CELL SHADES INDICATE HIGHER ACCURACY FOR CORRESPONDING TRAINING-TEST PAIRS IN EACH COLUMN. THE BASE MODEL IS QWEN2.5-VL-3B

No-Think RL fine-tuned Qwen2.5-VL-3B									
Test Train	CT	MRI	X-Ray	Ultrasound	Dermoscopy	Fundus	OCT	Microscopy	Overall
CT	98.27 ± 0.45	74.77 ± 1.04	85.33 ± 1.70	37.61 ± 2.05	69.07 ± 2.53	78.87 ± 2.46	87.26 ± 2.30	67.75 ± 2.75	74.87 ± 0.64
MRI	69.70 ± 1.56	99.61 ± 0.15	81.73 ± 1.89	34.91 ± 2.03	75.19 ± 2.34	80.51 ± 2.32	89.98 ± 2.00	67.48 ± 2.75	74.89 ± 0.65
X-Ray	80.10 ± 1.36	69.78 ± 1.14	95.79 ± 0.99	34.33 ± 2.05	71.29 ± 2.41	81.79 ± 2.28	83.14 ± 2.54	68.65 ± 2.79	73.11 ± 0.63
Ultrasound	56.40 ± 1.70	64.93 ± 1.18	80.25 ± 1.92	100.0 ± 0.00	68.38 ± 2.53	75.32 ± 2.60	76.30 ± 2.89	71.71 ± 2.66	74.16 ± 0.66
Dermoscopy	55.45 ± 1.70	66.48 ± 1.15	80.37 ± 1.95	37.42 ± 2.12	92.88 ± 1.38	71.86 ± 2.69	76.53 ± 2.83	67.12 ± 2.70	68.51 ± 0.69
Fundus	58.65 ± 1.68	66.08 ± 1.16	82.79 ± 1.83	34.33 ± 2.10	68.68 ± 2.49	93.81 ± 1.41	79.72 ± 2.71	65.86 ± 2.79	68.74 ± 0.69
OCT	80.38 ± 1.36	75.02 ± 1.05	86.81 ± 1.67	36.11 ± 2.05	72.21 ± 2.41	81.60 ± 2.28	99.88 ± 0.18	65.32 ± 2.79	74.67 ± 0.64
Microscopy	60.17 ± 1.73	66.59 ± 1.16	83.10 ± 1.86	36.60 ± 2.10	71.29 ± 2.45	77.05 ± 2.46	80.66 ± 2.71	97.66 ± 0.86	71.64 ± 0.67
Overall	69.89 ± 1.59	72.91 ± 1.08	84.52 ± 1.73	43.91 ± 2.14	73.62 ± 2.37	80.10 ± 2.41	84.18 ± 2.47	71.44 ± 2.65	72.57 ± 0.66

TABLE III

CROSS-MODALITY GENERALIZATION PERFORMANCE OF MED-R1 WITH THINK-AFTER RL POST-TRAINING. ACCURACY (%) ACROSS EIGHT MEDICAL IMAGING MODALITIES, WHERE ROWS INDICATE TRAINING MODALITIES AND COLUMNS TEST MODALITIES. DARKER CELL SHADES INDICATE HIGHER ACCURACY FOR CORRESPONDING TRAINING-TEST PAIRS IN EACH COLUMN. THE BASE MODEL IS QWEN2.5-VL-3B.

Think-after RL fine-tuned Qwen2.5-VL-3B									
Test Train	CT	MRI	X-Ray	Ultrasound	Dermoscopy	Fundus	OCT	Microscopy	Overall
CT	96.64 ± 0.62	72.53 ± 1.08	85.45 ± 1.67	36.31 ± 2.03	66.16 ± 2.53	79.78 ± 2.37	86.20 ± 2.30	68.20 ± 2.75	73.91 ± 0.65
MRI	63.65 ± 1.67	98.87 ± 0.26	81.11 ± 1.92	33.70 ± 2.03	71.82 ± 2.45	81.51 ± 2.32	86.91 ± 2.30	67.57 ± 2.70	73.14 ± 0.67
X-Ray	79.20 ± 1.42	72.70 ± 1.10	94.61 ± 1.08	31.58 ± 2.00	70.21 ± 2.45	80.60 ± 2.32	85.97 ± 2.30	68.65 ± 2.70	72.94 ± 0.66
Ultrasound	59.06 ± 1.70	66.23 ± 1.15	80.25 ± 1.95	99.37 ± 0.34	67.38 ± 2.53	74.95 ± 2.55	78.77 ± 2.77	67.93 ± 2.75	74.24 ± 0.64
Dermoscopy	56.77 ± 1.71	66.86 ± 1.15	80.37 ± 1.95	34.72 ± 2.07	89.51 ± 1.68	75.05 ± 2.55	78.66 ± 2.77	67.30 ± 2.75	68.65 ± 0.67
Fundus	58.01 ± 1.68	65.89 ± 1.16	81.30 ± 1.86	32.84 ± 2.03	68.68 ± 2.53	92.53 ± 1.55	79.36 ± 2.77	66.22 ± 2.79	68.10 ± 0.69
OCT	79.98 ± 1.37	75.45 ± 1.05	85.51 ± 1.73	34.14 ± 2.03	71.21 ± 2.45	81.69 ± 2.32	99.29 ± 0.53	66.94 ± 2.75	74.28 ± 0.65
Microscopy	59.27 ± 1.68	64.22 ± 1.19	81.11 ± 1.89	34.47 ± 2.05	63.86 ± 2.60	73.68 ± 2.64	78.42 ± 2.77	86.67 ± 2.03	67.71 ± 0.69
Overall	69.07 ± 1.62	72.84 ± 1.10	83.72 ± 1.76	42.14 ± 2.12	71.10 ± 2.53	79.97 ± 2.37	84.20 ± 2.47	69.93 ± 2.65	71.62 ± 0.66

CT - Computed Tomography; MRI - Magnetic Resonance Imaging; US - Ultrasound; Der - Dermoscopy; FP - Fundus Photography.

OCT - Optical Coherence Tomography; Micro - Microscopy Images; X-Ray - X-Ray Imaging

extracted answer matches the ground truth labels. Note that when there is any text outside the `<answer>` tag, i.e., an explicit thinking process exists, the extracted content will be null, and therefore the accuracy reward will be 0. Therefore, the model will be forced to generate only the answers.

C. Think-after Med-R1

As said in the previous section, removing both reasoning and format supervision during RL could sometimes improve performance. However, as medical AI systems must not

only achieve high accuracy but also provide reasoning that physicians can review and validate. To address this, we introduce a new reasoning protocol termed **Think-After**, in which the model first predicts the answer and then generates a post-hoc rationale explaining that decision. This design preserves interpretability while minimizing the instability introduced by lengthy reasoning chains. Concretely, the instruction prompt is revised as: {Question}. Output the single-letter choice (A, B, C, D,...) in `<answer>...</answer>` tags. Then provide

TABLE IV

PERFORMANCE COMPARISON ACROSS EIGHT MEDICAL MODALITIES. OUR GRPO-FINETUNED MODEL OUTPERFORMS ZERO-SHOT GENERAL-PURPOSE VLMS, MEDICAL-DOMAIN VLMS, AND SUPERVISED FINE-TUNING BASELINES, WHILE MAINTAINING SCALABILITY. THE BEST AND SECOND-BEST PERFORMANCES PER COLUMN ARE HIGHLIGHTED IN **RED** AND **BLUE**. MODALITY ABBREVIATIONS: CT – COMPUTED TOMOGRAPHY; MRI – MAGNETIC RESONANCE IMAGING; US – ULTRASOUND; DER – DERMOSCOPY; FP – FUNDUS PHOTOGRAPHY; OCT – OPTICAL COHERENCE TOMOGRAPHY; MICRO – MICROSCOPY; X-RAY – X-RAY IMAGING.

Modality Methods \	CT	MRI	X-Ray	Ultrasound	Dermoscopy	Fundus	OCT	Microscopy	Overall
Zero-shot VLMS									
BLIP-2 [†] [15]	56.74	41.32	67.58	37.27	40.65	46.24	68.08	50.40	51.04
InstructBLIP [†] [27]	28.72	33.15	61.04	41.25	62.22	50.31	42.59	46.29	45.70
LLaVA [†] [28]	17.73	26.72	30.70	18.66	49.74	47.11	33.73	28.87	31.66
LLaMA Adapter v2 [†] [29]	21.41	26.63	46.44	34.05	51.76	50.74	33.00	38.66	37.83
MiniGPT-4 [†] [30]	22.81	27.48	38.30	25.50	40.25	38.33	31.40	36.23	32.54
InternVL2 [31]	40.20	58.10	57.90	49.10	51.90	53.20	59.10	64.00	54.19
Qwen2-VL-2B [3]	45.10	38.57	39.32	30.86	35.83	43.17	35.14	36.85	38.11
Qwen2-VL-7B [3]	61.46	45.77	64.27	36.01	49.08	59.84	59.32	61.08	54.60
Qwen2-VL-72B [32]	67.97	69.39	77.21	51.39	65.31	72.58	72.76	67.83	68.05
Qwen2.5-VL-3B [33]	53.87	54.23	61.84	32.69	52.94	62.47	56.23	59.64	54.24
Qwen2.5-VL-7B [33]	60.44	58.44	73.99	30.66	62.48	67.30	61.20	67.84	60.29
Qwen2.5-VL-72B [33]	66.18	68.74	77.59	49.81	69.75	71.04	69.22	69.37	67.71
Zero-shot Medical VLMS									
LLaVA-Med [†] [8]	18.69	27.47	30.68	29.88	44.95	39.03	34.61	33.29	32.33
RadFM [†] [34]	27.56	24.06	30.95	16.57	39.21	36.89	32.80	27.97	29.50
Med-Flamingo [†] [6]	38.47	40.56	30.34	24.64	32.43	30.12	26.51	19.93	30.38
MedViNT [†] [7]	40.74	43.10	55.10	41.26	29.11	31.84	23.26	32.00	37.05
HuatuoGPT-Vision [9]	35.30	40.40	41.50	60.10	53.10	51.40	59.30	62.30	50.43
HealthGPT [35]	35.50	78.50	81.90	51.40	64.90	54.60	89.30	88.20	68.04
Fine-tuned VLMS									
Qwen2-VL-2B (SFT)	51.74	52.83	65.57	47.65	51.91	52.26	53.99	56.58	54.07
Qwen2.5-VL-3B (SFT)	56.06	60.81	69.23	41.77	60.11	69.19	63.95	65.66	60.85
Qwen2-VL-2B (Think)	66.30	71.67	77.73	57.31	72.33	71.20	71.96	70.80	69.91
Qwen2-VL-2B (Nothink)	72.19	74.37	78.37	54.43	74.73	75.07	76.59	74.13	72.49
Qwen2.5-VL-3B (Think)	73.46	68.77	83.72	45.21	68.88	77.40	82.18	69.47	71.14
Qwen2.5-VL-3B (Think-after)	69.07	72.84	83.72	42.14	71.10	79.97	84.20	69.93	71.62
Qwen2.5-VL-3B (Nothink)	69.89	72.91	84.52	43.91	73.62	80.10	84.18	71.44	72.57

the reasoning step by step to explain why you chose this answer. where {Question} is replaced by each specific VQA item. By separating answer prediction and rationale generation, we reduce interference between reasoning and decision processes, achieving balanced trade-off between accuracy and interpretability.

IV. EXPERIMENT & RESULTS

A. Setup

Datasets. We adopt the VQA data from the open-access part of the OmniMedVQA benchmark [36], which consists of a total of 82,059 images and 88,996 vision question answering pairs. OmniMedVQA includes VQA pairs from eight imaging modalities: CT (15,808), MRI (31,877), X-Ray (7,916), Ultrasound (10,991), Dermoscopy (6,679), Fundus (5,398), OCT (4,646), and Microscopy (5,680). It is also categorized into five VQA question types, including Anatomy Identification (16,448), Disease Diagnosis (55,387), Lesion Grading (2,098), Modality Recognition (11,565), and Other Biological Attributes (3,498). We split the dataset into training and test sets following an 80-20 ratio for each setting.

Implementation Details Training is conducted on HGX H100 [37] server with 2xH100 GPUs (80GB VRAM) using

PyTorch [38] and FlashAttention-2 [39] for optimized efficiency. We initialize from Qwen2-VL-2B-Instruct [3] with full parameter tuning, employing per-GPU batch size 1 (effective batch size 4 via 2-step gradient accumulation) and bfloat16 mixed precision. Input sequences combine visual embeddings from 328×328 resolution images (max 401k pixels) with textual prompts truncated to 1,024 tokens. The GRPO policy generates four candidate rationales per sample, with a sampling temperature of $\tau = 0.7$. Each training is run for one epoch.

Task setting. We evaluate our approach in two distinct generalization settings using the OmniMedVQA dataset [36]: cross-modality generalization and cross-task generalization.

- **Cross-modality generalization:** We train our model on a single modality at a time (out of 8 available modalities) and evaluate its performance on the other seven modalities.
- **Cross-task generalization:** We identify 5 distinct task types within the dataset and adopt the same train-test partitioning strategy as in the cross-modality setting, training on one task and evaluating on the other four.

We focus on VQA, which integrates core vision–language abilities such as classification, grounding, and reasoning into a unified framework, making it a representative precursor to detection or captioning tasks.

TABLE V

CROSS-TASK GENERALIZATION OF MED-R1: PERFORMANCE IS EVALUATED ACROSS FIVE CLINICAL REASONING TASK TYPES (ROWS: TRAINING TASKS, COLUMNS: TEST TASKS), WITH DARKER CELL SHADING INDICATING STRONGER GENERALIZATION. RESULTS DEMONSTRATE THAT DOMAIN-SPECIFIC TRAINING (E.G., DISEASE DIAGNOSIS) PRESERVES IN-TASK EXPERTISE WHILE MAINTAINING ADAPTABILITY TO UNSEEN TASKS, PARTICULARLY FOR MODALITY-AGNOSTIC SKILLS LIKE MODALITY RECOGNITION. THE BASE MODEL IS QWEN2.5-VL-3B.

RL fine-tuned Qwen2.5-VL-3B						
Train \ Test	Anatomy Identification	Disease Diagnosis	Lesion Grading	Modality Recognition	Other Attributes	Overall
Anatomy Identification	94.65 \pm 0.75	61.87 \pm 0.90	63.30 \pm 4.59	96.66 \pm 0.73	78.69 \pm 3.05	79.04 \pm 0.65
Disease Diagnosis	43.83 \pm 1.67	97.74 \pm 0.28	79.82 \pm 3.67	96.66 \pm 0.73	87.78 \pm 2.41	81.16 \pm 0.49
Lesion Grading	47.10 \pm 1.71	59.33 \pm 0.93	88.99 \pm 2.98	96.03 \pm 0.77	69.03 \pm 3.41	72.10 \pm 0.70
Modality Recognition	45.96 \pm 1.67	58.63 \pm 0.91	67.89 \pm 4.36	99.08 \pm 0.40	69.46 \pm 3.41	68.20 \pm 0.71
Other Attributes	44.04 \pm 1.68	60.09 \pm 0.92	60.09 \pm 4.59	95.74 \pm 0.82	94.74 \pm 1.63	70.94 \pm 0.70
Overall	55.12 \pm 0.75	67.53 \pm 0.39	72.02 \pm 1.86	96.83 \pm 0.31	79.94 \pm 1.32	74.29 \pm 0.65

TABLE VI

NO-THINK CROSS-TASK GENERALIZATION OF MED-R1: PERFORMANCE IS EVALUATED ACROSS FIVE CLINICAL REASONING TASK TYPES (ROWS: TRAINING TASKS, COLUMNS: TEST TASKS), WITH DARKER CELL SHADING INDICATING STRONGER GENERALIZATION.

No-Think RL fine-tuned Qwen2.5-VL-3B						
Train \ Test	Anatomy Identification	Disease Diagnosis	Lesion Grading	Modality Recognition	Other Attributes	Overall
Anatomy Identification	96.85 \pm 0.57	63.86 \pm 0.90	79.59 \pm 3.78	96.82 \pm 0.69	77.41 \pm 3.12	82.91 \pm 0.64
Disease Diagnosis	44.82 \pm 1.73	98.78 \pm 0.21	85.78 \pm 3.33	95.82 \pm 0.82	90.91 \pm 2.13	83.22 \pm 0.48
Lesion Grading	44.61 \pm 1.70	60.27 \pm 0.91	97.02 \pm 1.61	95.90 \pm 0.79	82.10 \pm 2.84	75.98 \pm 0.70
Modality Recognition	47.07 \pm 1.71	59.58 \pm 0.91	75.92 \pm 3.90	99.75 \pm 0.19	81.53 \pm 2.84	72.77 \pm 0.70
Other Attributes	43.98 \pm 1.71	61.11 \pm 0.90	61.70 \pm 4.59	96.07 \pm 0.77	95.60 \pm 1.49	71.69 \pm 0.71
Overall	55.46 \pm 0.77	68.72 \pm 0.39	80.00 \pm 1.67	96.87 \pm 0.31	85.51 \pm 1.16	77.31 \pm 0.62

Baseline Methods & Evaluation Metric.

We report our results by separating the baselines into three groups. Zero-shot VLMs are models pre-trained for general-purpose VQA without medical adaptation. Medical VLMs are models pre-trained on medical data specifically for medical VQA. Fine-tuned VLMs are models trained on OmniMedVQA using supervised fine-tuning and RL fine-tuning. We evaluate model performance using **VQA choice accuracy**, the standard metric for medical VQA, where the model selects the correct answer from K clinically validated options. Given an image I , a question Q , and candidate answers $\{A_k\}_{k=1}^K$, accuracy is defined as:

$$\text{Accuracy} = \frac{1}{N} \sum_{i=1}^N \mathbb{I}(\hat{y}_i = y_i), \quad (2)$$

where N is the total number of test cases, \hat{y}_i is the predicted answer index, y_i the ground truth, and \mathbb{I} the indicator function (1 if correct, 0 otherwise).

To assess result reliability, we computed **95% bootstrap confidence intervals (CIs)** for all model variants across modalities and tasks. Each experiment performed 10,000 bootstrap resamplings of binary accuracy labels to estimate the mean and confidence bounds, reporting $\text{mean} \pm \text{half-width}$ for each model.

All fine-tuned VLM results (SFT, GRPO+Think, GRPO+Think-After, and GRPO+No-Think) are computed under the identical averaging protocol—macro-averaged accuracy across all cross-modality training–testing pairs—to ensure fair and consistent comparison.

B. Cross-Modality Generalization

We comprehensively evaluate Med-R1’s adaptability across **eight** medical imaging modalities, including Computed To-

mography, Magnetic Resonance Imaging, Ultrasound, Dermoscopy, Fundus Photography, Optical Coherence Tomography, Microscopy Images, and X-ray Imaging. Our experiments focus on two key aspects: (1) cross-modal generalization, where the model is trained on one modality and tested on another, and (2) comparative performance against other popular VLMs and medical-specific VLMs evaluated using zero-shot and SFT.

Results on generalization. To evaluate Med-R1’s cross-modality generalization, we measure its accuracy across eight distinct medical imaging modalities (Table I). Overall row and column summarize the model’s average performance across training and test domains, providing insights into its generalization ability. Med-R1 achieves a strong overall accuracy of 69.91%, demonstrating its ability to generalize across diverse medical imaging modalities. Notably, models trained on CT, MRI, and X-Ray exhibit the highest generalization capability, with overall scores of 71.44%, 71.26%, and 72.35%, respectively. In contrast, models trained on Fundus Photography and Microscopy images show lower generalization, with 67.67% and 67.54% overall accuracy, indicating that certain modality-specific features (e.g., texture-based imaging in US and Micro) may not transfer as effectively to other domains. Importantly, the overall test accuracy of 69.91% highlights Med-R1’s ability to perform well across unseen imaging modalities, despite being trained on a single domain at a time. This result underscores the effectiveness of reinforcement learning in enhancing cross-modality transfer, allowing the model to maintain robust performance without requiring extensive retraining for each medical imaging modality.

Comparison to zero-shot and SFT evaluations with other VLMs. As demonstrated in Table IV, Med-R1 demonstrates its superiority across all eight medical imaging modalities while

TABLE VII

THINK-AFTER CROSS-TASK GENERALIZATION OF MED-R1: PERFORMANCE IS EVALUATED ACROSS FIVE CLINICAL REASONING TASK TYPES (ROWS: TRAINING TASKS, COLUMNS: TEST TASKS), WITH DARKER CELL SHADING INDICATING STRONGER GENERALIZATION.

Think-After fine-tuned Qwen2.5-VL-3B						
Train \ Test	Anatomy Identification	Disease Diagnosis	Lesion Grading	Modality Recognition	Other Attributes	Overall
Anatomy Identification	95.22 ± 0.74	60.62 ± 0.90	65.83 ± 4.36	96.57 ± 0.73	81.53 ± 2.91	79.95 ± 0.65
Disease Diagnosis	43.11 ± 1.68	97.86 ± 0.27	81.65 ± 3.67	95.99 ± 0.77	92.33 ± 1.99	82.19 ± 0.49
Lesion Grading	43.56 ± 1.70	59.78 ± 0.92	85.55 ± 3.21	96.20 ± 0.77	78.55 ± 3.05	72.73 ± 0.71
Modality Recognition	44.73 ± 1.71	58.82 ± 0.93	68.12 ± 4.47	98.87 ± 0.44	78.12 ± 3.05	69.73 ± 0.71
Other Attributes	45.21 ± 1.67	59.65 ± 0.90	67.43 ± 4.36	95.74 ± 0.82	95.74 ± 1.49	72.75 ± 0.71
Overall	54.36 ± 0.75	67.34 ± 0.40	73.72 ± 1.86	96.67 ± 0.32	85.26 ± 1.18	75.47 ± 0.63

TABLE VIII

PERFORMANCE COMPARISON OF VLMs ON FIVE MEDICAL VQA TASKS: GRPO FINE-TUNING OUTPERFORMS ZERO-SHOT AND SFT BASELINES ACROSS DIVERSE REASONING TASKS. PERFORMANCE IS EVALUATED ON FIVE CLINICAL REASONING TYPES (COLUMNS) ACROSS THREE MODEL CATEGORIES: GENERAL-PURPOSE VLMs (ZERO-SHOT), MEDICAL VLMs (ZERO-SHOT), AND FINE-TUNED VLMs. THE BEST AND SECOND-BEST PERFORMANCES ARE MARKED IN RED AND BLUE.

Methods \ Types	Anatomy Identification	Disease Diagnosis	Lesion Grading	Modality Recognition	Other Attributes	Overall
Zero-shot VLMs						
BLIP-2 [†] [15]	44.39	44.51	29.03	68.19	67.95	48.12
InstructBLIP [†] [27]	44.35	32.29	59.25	75.27	23.72	40.40
LLaVA [†] [28]	25.86	29.10	43.95	21.36	31.90	27.96
LLaMA Adapter v2 [†] [29]	33.72	31.19	41.99	37.29	34.22	32.82
MiniGPT-4 [†] [30]	28.88	30.47	34.56	26.43	30.36	29.74
Qwen2-VL-2B [3]	30.70	36.53	43.58	59.90	42.19	42.58
Qwen2-VL-7B [3]	42.57	48.83	52.06	84.74	59.66	57.57
Qwen2-VL-72B [32]	56.41	65.71	62.15	98.11	80.53	72.58
Qwen2.5-VL-3B [33]	35.23	50.45	52.79	85.23	54.77	55.69
Qwen2.5-VL-7B [33]	41.00	61.32	54.13	97.78	70.45	64.94
Qwen2.5-VL-72B [33]	57.22	62.55	60.32	98.20	77.41	71.14
Zero-shot Medical VLMs						
LLaVA-Med [†] [8]	29.53	29.22	34.18	26.93	33.08	29.25
RadFM [†] [34]	13.31	21.69	30.35	26.64	43.85	26.99
Med-Flamingo [†] [6]	24.93	38.90	30.74	30.19	14.18	34.03
MedVInT [†] [7]	40.26	35.78	12.77	68.10	30.30	40.04
Fine-tuned VLMs						
Qwen2-VL-2B (SFT)	53.97	51.62	60.71	86.77	63.91	63.39
Qwen2.5-VL-3B (SFT)	54.91	57.75	64.04	84.95	71.56	66.64
Qwen2-VL-2B (Think)	62.88	66.08	65.87	98.24	80.14	74.64
Qwen2-VL-2B (Nothink)	63.74	66.32	66.33	98.44	81.31	75.22
Qwen2.5-VL-3B (Think)	55.12	67.53	72.02	96.83	79.94	74.29
Qwen2.5-VL-3B (Think-after)	54.36	67.34	73.72	96.67	85.26	75.47
Qwen2.5-VL-3B (Nothink)	55.47	68.72	80.00	96.87	85.51	77.31

maintaining exceptional parameter efficiency. For zero-shot results, each cell denotes the zero-shot evaluation accuracy of the model on the particular modality. For all the fine-tuned VLM results, each cell represents the overall accuracy, reflecting the average generalization performance of the given modality when evaluated using models that were separately fine-tuned on each of the eight training modalities. Against general-purpose VLMs, our 2B-parameter model achieves 69.91% overall accuracy, surpassing the 72B-parameter Qwen2-VL by 1.86%—a notable result given the 36× parameter disparity. This advantage amplifies in critical diagnostic tasks: Med-R1 attains 71.67% accuracy in MRI compared to Qwen2-VL-72B's 69.39%, and achieves 72.33% versus 65.31% in dermoscopy, challenging the prevailing scale-equals-performance paradigm. The limitations of specialized medical VLMs become evident through Med-Flamingo's 30.38% average accuracy, which Med-

R1 outperforms by 39.53%. This stark contrast underscores the ineffectiveness of narrow medical pretraining compared to our RL-driven adaptation strategy. When compared to supervised fine-tuning approaches, GRPO delivers 15.84% accuracy gains over SFT-tuned Qwen2-VL-2B (69.91% vs. 54.07%), with particularly significant improvements in CT interpretation (66.30% vs. 51.74%) and OCT analysis (71.96% vs. 53.99%).

C. Cross-Task Generalization

We also evaluate Med-R1's generalization across **five** important clinical tasks [36]: Anatomy Identification, Disease Diagnosis, Lesion Grading, Modality Recognition, and Other Attributes. Similar to subsection IV-B, we focus our evaluation on two aspects: cross-modality generalization and comparison against SFT and zero-shot with other VLMs.

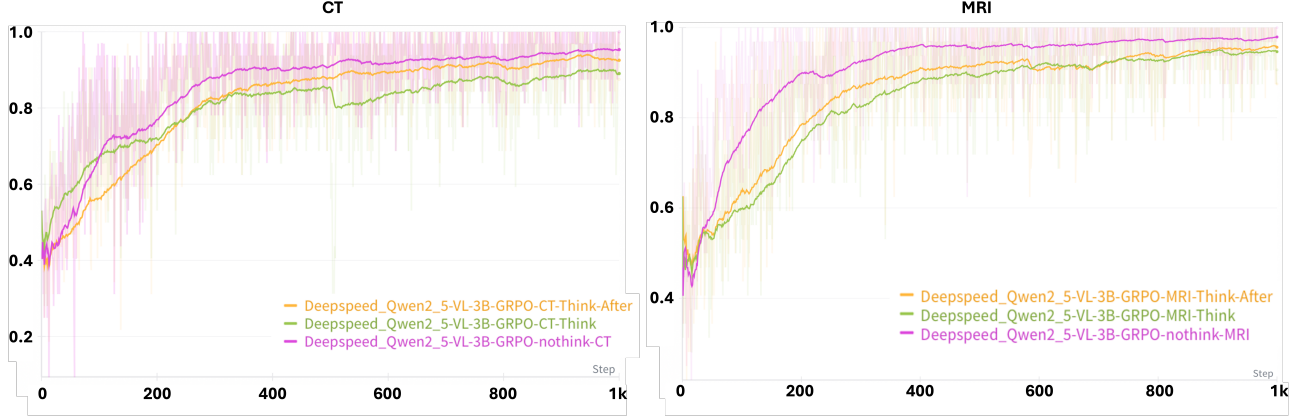


Fig. 3. Training accuracy-reward curves of the Think, No-Think, and Think-After models on CT and MRI datasets.



Fig. 4. Cross-modality accuracy difference between No-Thinking-Med-R1 and Med-R1. Each cell shows the performance gap (%) when trained on one modality (y-axis) and evaluated on others (x-axis). Red indicates improvement; blue indicates degradation.



Fig. 5. Cross-task accuracy difference between No-Thinking-Med-R1 and Med-R1. Each cell shows the performance gap (%) when trained on one task (y-axis) and tested on another (x-axis). Red indicates improvement; blue indicates degradation.

Results on generalization. As shown in Table V, models trained on “disease diagnosis” data achieve the best generalization, with 81.64% overall accuracy. This suggests that disease diagnosis encompasses diverse feature representations that transfer well across tasks, likely due to its reliance on both anatomical and pathological cues. In contrast, models trained on “modality recognition” exhibit strong generalization in task-agnostic settings (98.24% in the “modality recognition” column), indicating that learning modality distinctions aids in extracting transferable image features. However, training on “lesion grading” leads to high in-task performance (86.24%) but relatively lower transferability, implying that this task captures more specialized features that do not generalize as effectively. These results highlight the trade-off between specialization and adaptability, emphasizing the importance of task selection when designing models for broad medical applications.

Comparison to zero-shot and SFT evaluations with other VLMs. Table VIII shows the comparison results with other popular VLMs evaluated with zero-shot and SFT. For zero-shot results, each cell denotes the zero-shot evaluation accuracy of the model on the particular task. For the fine-tuned VLM results (last two rows), each cell represents the overall accuracy, reflecting the average generalization performance of the given task when evaluated using models that were separately fine-tuned on each of the five training tasks. First of all, the results clearly show that Med-R1 outperforms all other popular VLMs’ zero-shot generalization. Remarkably, Med-R1 even outperforms Qwen2-VL-72B (74.64% vs. 72.58%), a model with **70 billion** more parameters. More importantly, this suggests that RL can effectively elevate small models with moderate capacity, opening doors for many real-world applications where resource is a constraint. In contrast, the

average generalization with the identical base model trained with SFT is merely 63.39%, 11.25% below Med-R1, further demonstrating the strong generalization capability of Med-R1.

D. Analysis of No-Think

We present the results of No-Thinking-Med-R1 in this section. Cross-task performance is shown in Table VI, and cross-modality performance is shown in Table II. Overall, No-Thinking-Med-R1 achieves stronger in-domain performance across all settings compared to Med-R1, suggesting that removing explicit reasoning generation may lead to more effective task-specific learning. To assess generalization, we compare Med-R1 and No-Thinking-Med-R1 across modalities and tasks. As visualized in Figure 4 and Figure 5, No-Thinking-Med-R1 consistently outperforms Med-R1 in cross-modality settings. In cross-task scenarios, however, the results are more mixed—showing gains in some tasks and declines in others. These findings reinforce the practical motivation behind Med-R1. In clinical domains, acquiring high-quality CoT supervision is prohibitively costly and often impractical. While reasoning improves performance in general domains, our results show that this does not necessarily hold in medical settings, where unsupervised rationales may become unreliable under domain shift. Med-R1 demonstrates that even without reasoning supervision, RL can offer a robust and efficient path for adapting VLMs to medicine.

E. Analysis of Think-after

We introduce the **Think-After** strategy primarily to address the practical need for achieving both high accuracy and interpretable reasoning in medical VLMs (Table VII, Table III). Rather than serving solely as a control experiment, Think-After is designed to meet the dual objective of preserving predictive performance while providing reasoning traces that clinicians can review and validate.

Beyond satisfying the need for both accuracy and interpretability, Think-After also provides insight into why the *No-Thinking* strategy sometimes outperforms the conventional *Thinking* approach. As shown in Figure 3, Think-After achieves faster convergence and higher accuracy rewards than the Thinking variant, suggesting that generating reasoning tokens *before* the answer may disrupt the autoregressive generation process and hinder optimization. However, Think-After still performs slightly below No-Thinking, indicating that additional mechanisms—such as residual contextual coupling or reasoning-token noise—may also contribute to the performance gap. While Think-After does not completely resolve the question of why No-Thinking surpasses both pre- and post-answer reasoning, it fulfills the essential requirement of combining strong accuracy with interpretable outputs, and simultaneously offers valuable clues toward understanding the dynamics between reasoning generation and performance in medical VLMs.

F. Reader Study

To further assess interpretability and clinical relevance, we conducted a reader study with three researchers experienced in

TABLE IX

READER STUDY RESULTS. THREE READERS INDEPENDENTLY EVALUATED 100 CORRECTLY ANSWERED VQA SAMPLES FOR FACTUAL CORRECTNESS (QUALITY, 1–5) AND REASONING-ANSWER CONSISTENCY (CONSISTENCY, %).

Reader	Quality	Consistency (%)
A	4.23	93.0
B	4.19	92.0
C	4.34	95.0
Mean	4.25	93.3

Quality reflects factual and clinical correctness of model answers; Consistency measures logical alignment between reasoning and answers.

medical imaging and vision–language models. Each independently evaluated 100 representative VQA samples generated by different model variants, covering diverse imaging modalities and reasoning types (Table IX). Evaluations focused on (1) the factual and clinical correctness of model answers and (2) the logical consistency between the reasoning (“Think”) and the predicted answer (“Answer”). Across readers, the *Think-After* model achieved the highest agreement and was consistently judged to produce reasoning that was both coherent and clinically sound, demonstrating improved interpretability and reasoning reliability for medical decision-support applications.

G. Limitations and Future Work.

This work marks an initial step in applying RL to medical vision–language models. We adopt a frame-level VQA setting for consistent evaluation across modalities, but this simplifies the real-world complexity of medical imaging. In practice, CT and MRI are volumetric, and ultrasound is dynamic, requiring reasoning across slices and time. Another limitation lies in the reasoning supervision and data scale. Our findings suggest that the “No-Thinking” model occasionally outperforms reasoning-enabled variants, which may stem from the limited availability of high-quality medical reasoning data.

In domains where clinically faithful chain-of-thought (CoT) annotations are scarce, the model may not learn to benefit from explicit reasoning, leading the reasoning process to introduce noise rather than insight. We believe this reflects a broader limitation of current medical datasets rather than of reasoning itself. Future work should explore scaling up medically grounded CoT data and aligning RL rewards with clinically validated reasoning quality to fully realize the benefits of explicit reasoning. Future directions also include extending Med-R1 to support multi-frame or volumetric inputs, incorporating patient context, and investigating more advanced reasoning frameworks for clinical deployment.

V. CONCLUSION

We present **Med-R1**, a reinforcement learning–enhanced vision–language model for improving medical reasoning across diverse imaging modalities and clinical tasks. Leveraging GRPO-based post-training, Med-R1 achieves strong cross-modality and cross-task generalization, surpassing the limits of supervised fine-tuning. Despite its compact 3B scale, Med-R1 performs competitively with or better than larger medical and general VLMs, while remaining efficient for deployment.

Through systematic analysis, we find that removing explicit reasoning (*No-Think*) improves convergence and generalization, suggesting that reasoning *quality*, not quantity, drives medical performance. To balance interpretability and accuracy, we introduce the *Think-After* strategy, which decouples reasoning from answer generation and enhances clinical transparency without compromising accuracy. Overall, Med-R1 establishes a scalable framework for reinforcement learning in medical VLMs and offers new insights into how reasoning dynamics interact with domain generalization, paving the way toward reliable and interpretable medical AI systems.

REFERENCES

- [1] A. Hurst, A. Lerer, A. P. Goucher, A. Perelman, A. Ramesh, A. Clark, A. Ostrow, A. Welihinda, A. Hayes, A. Radford *et al.*, “Gpt-4o system card,” *arXiv preprint arXiv:2410.21276*, 2024.
- [2] G. Team, “Gemini 1.5: Unlocking multimodal understanding across millions of tokens of context,” 2024. [Online]. Available: <https://arxiv.org/abs/2403.05530>
- [3] J. Bai, S. Bai, Y. Chu, Z. Cui, K. Dang, X. Deng, Y. Fan, W. Ge, Y. Han, F. Huang *et al.*, “Qwen technical report,” *arXiv preprint arXiv:2309.16609*, 2023.
- [4] W. Chen, X. Ma, X. Wang, and W. W. Cohen, “Program of thoughts prompting: Disentangling computation from reasoning for numerical reasoning tasks,” *arXiv preprint arXiv:2211.12588*, 2022.
- [5] J. Achiam, S. Adler, S. Agarwal, L. Ahmad, I. Akkaya, F. L. Aleman, D. Almeida, J. Alteneschmidt, S. Altman, S. Anadkat *et al.*, “Gpt-4 technical report,” *arXiv preprint arXiv:2303.08774*, 2023.
- [6] M. Moor, Q. Huang, S. Wu, M. Yasunaga, Y. Dalmia, J. Leskovec, C. Zakra, E. P. Reis, and P. Rajpurkar, “Med-flamingo: a multimodal medical few-shot learner,” in *Machine Learning for Health (ML4H)*. PMLR, 2023, pp. 353–367.
- [7] X. Zhang, C. Wu, Z. Zhao, W. Lin, Y. Zhang, Y. Wang, and W. Xie, “Pmc-vqa: Visual instruction tuning for medical visual question answering,” *arXiv preprint arXiv:2305.10415*, 2023.
- [8] C. Li, C. Wong, S. Zhang, N. Usuyama, H. Liu, J. Yang, T. Naumann, H. Poon, and J. Gao, “Llava-med: Training a large language-and-vision assistant for biomedicine in one day,” *Advances in Neural Information Processing Systems*, vol. 36, pp. 28541–28564, 2023.
- [9] J. Chen, C. Gui, R. Ouyang, A. Gao, S. Chen, G. H. Chen, X. Wang, R. Zhang, Z. Cai, K. Ji *et al.*, “Huatuogpt-vision, towards injecting medical visual knowledge into multimodal llms at scale,” *arXiv preprint arXiv:2406.19280*, 2024.
- [10] Y. Li, Y. Lai, M. Thor, D. Marshall, Z. Buchwald, D. S. Yu, and X. Yang, “Towards universal text-driven ct image segmentation,” *arXiv preprint arXiv:2503.06030*, 2025.
- [11] T. Chu, Y. Zhai, J. Yang, S. Tong, S. Xie, D. Schuurmans, Q. V. Le, S. Levine, and Y. Ma, “Sft memorizes, rl generalizes: A comparative study of foundation model post-training,” *arXiv preprint arXiv:2501.17161*, 2025.
- [12] Z. Shao, P. Wang, Q. Zhu, R. Xu, J. Song, X. Bi, H. Zhang, M. Zhang, Y. Li, Y. Wu *et al.*, “Deepseekmath: Pushing the limits of mathematical reasoning in open language models,” *arXiv preprint arXiv:2402.03300*, 2024.
- [13] J. Schulman, F. Wolski, P. Dhariwal, A. Radford, and O. Klimov, “Proximal policy optimization algorithms,” *arXiv preprint arXiv:1707.06347*, 2017.
- [14] A. Radford, J. W. Kim, C. Hallacy, A. Ramesh, G. Goh, S. Agarwal, G. Sastry, A. Askell, P. Mishkin, J. Clark *et al.*, “Learning transferable visual models from natural language supervision,” in *International conference on machine learning*. PMLR, 2021, pp. 8748–8763.
- [15] J. Li, D. Li, S. Savarese, and S. Hoi, “Blip-2: Bootstrapping language-image pre-training with frozen image encoders and large language models,” in *International conference on machine learning*. PMLR, 2023, pp. 19730–19742.
- [16] L. Ouyang, J. Wu, X. Jiang, D. Almeida, C. Wainwright, P. Mishkin, C. Zhang, S. Agarwal, K. Slama, A. Ray *et al.*, “Training language models to follow instructions with human feedback,” *Advances in neural information processing systems*, vol. 35, pp. 27730–27744, 2022.
- [17] Y. Bai, S. Kadavath, S. Kundu, A. Askell, J. Kernion, A. Jones, A. Chen, A. Goldie, A. Mirhoseini, C. McKinnon *et al.*, “Constitutional ai: Harmlessness from ai feedback,” *arXiv preprint arXiv:2212.08073*, 2022.
- [18] J. Wei, X. Wang, D. Schuurmans, M. Bosma, F. Xia, E. Chi, Q. V. Le, D. Zhou *et al.*, “Chain-of-thought prompting elicits reasoning in large language models,” *Advances in neural information processing systems*, vol. 35, pp. 24824–24837, 2022.
- [19] W. Li, C. Qu, X. Chen, P. R. Bassi, Y. Shi, Y. Lai, Q. Yu, H. Xue, Y. Chen, X. Lin *et al.*, “Abdomenatlas: A large-scale, detailed-annotated, & multi-center dataset for efficient transfer learning and open algorithmic benchmarking,” *Medical Image Analysis*, vol. 97, p. 103285, 2024.
- [20] J. Pan, C. Liu, J. Wu, F. Liu, J. Zhu, H. B. Li, C. Chen, C. Ouyang, and D. Rueckert, “Medvlm-r1: Incentivizing medical reasoning capability of vision-language models (vlms) via reinforcement learning,” *arXiv preprint arXiv:2502.19634*, 2025.
- [21] W. Huang, B. Jia, Z. Zhai, S. Cao, Z. Ye, F. Zhao, Z. Xu, Y. Hu, and S. Lin, “Vision-r1: Incentivizing reasoning capability in multimodal large language models,” 2025. [Online]. Available: <https://arxiv.org/abs/2503.06749>
- [22] Z. Shao, P. Wang, Q. Zhu, R. Xu, J. Song, X. Bi, H. Zhang, M. Zhang, Y. K. Li, Y. Wu, and D. Guo, “Deepseekmath: Pushing the limits of mathematical reasoning in open language models,” 2024. [Online]. Available: <https://arxiv.org/abs/2402.03300>
- [23] S. Bai, K. Chen, X. Liu, J. Wang, W. Ge, S. Song, K. Dang, P. Wang, S. Wang, J. Tang, H. Zhong, Y. Zhu, M. Yang, Z. Li, J. Wan, P. Wang, W. Ding, Z. Fu, Y. Xu, J. Ye, X. Zhang, T. Xie, Z. Cheng, H. Zhang, Z. Yang, H. Xu, and J. Lin, “Qwen2.5-vl technical report,” 2025. [Online]. Available: <https://arxiv.org/abs/2502.13923>
- [24] S. Kullback and R. A. Leibler, “On information and sufficiency,” *Annals of Mathematical Statistics*, vol. 22, no. 1, pp. 79–86, 1951.
- [25] D. Guo, D. Yang, H. Zhang, J. Song, R. Zhang, R. Xu, Q. Zhu, S. Ma, P. Wang, X. Bi *et al.*, “Deepseek-r1: Incentivizing reasoning capability in llms via reinforcement learning,” *arXiv preprint arXiv:2501.12948*, 2025.
- [26] M. Li, S. Zhao, J. Zhong, Y. Lai, and K. Zhang, “Cls-rl: Image classification with rule-based reinforcement learning,” *arXiv preprint arXiv:2503.16188*, 2025.
- [27] W. Dai, J. Li, D. Li, A. M. H. Tiong, J. Zhao, W. Wang, B. Li, P. Fung, and S. Hoi, “Instructblip: Towards general-purpose vision-language models with instruction tuning,” 2023. [Online]. Available: <https://arxiv.org/abs/2305.06500>
- [28] H. Liu, C. Li, Q. Wu, and Y. J. Lee, “Visual instruction tuning,” *Advances in neural information processing systems*, vol. 36, pp. 34892–34916, 2023.
- [29] P. Gao, J. Han, R. Zhang, Z. Lin, S. Geng, A. Zhou, W. Zhang, P. Lu, C. He, X. Yue *et al.*, “Llama-adapter v2: Parameter-efficient visual instruction model,” *arXiv preprint arXiv:2304.15010*, 2023.
- [30] D. Zhu, J. Chen, X. Shen, X. Li, and M. Elhoseiny, “Minigpt-4: Enhancing vision-language understanding with advanced large language models,” *arXiv preprint arXiv:2304.10592*, 2023.
- [31] Z. Chen, W. Wang, Y. Cao, Y. Liu, Z. Gao, E. Cui, J. Zhu, S. Ye, H. Tian, Z. Liu *et al.*, “Expanding performance boundaries of open-source multimodal models with model, data, and test-time scaling,” *arXiv preprint arXiv:2412.05271*, 2024.
- [32] P. Wang, S. Bai, S. Tan, S. Wang, Z. Fan, J. Bai, K. Chen, X. Liu, J. Wang, W. Ge *et al.*, “Qwen2-vl: Enhancing vision-language model’s perception of the world at any resolution,” *arXiv preprint arXiv:2409.12191*, 2024.
- [33] S. Bai, K. Chen, X. Liu, J. Wang, W. Ge, S. Song, K. Dang, P. Wang, S. Wang, J. Tang *et al.*, “Qwen2. 5-vl technical report,” *arXiv preprint arXiv:2502.13923*, 2025.
- [34] C. Wu, X. Zhang, Y. Zhang, Y. Wang, and W. Xie, “Towards generalist foundation model for radiology by leveraging web-scale 2d&3d medical data,” *arXiv preprint arXiv:2308.02463*, 2023.
- [35] T. Lin, W. Zhang, S. Li, Y. Yuan, B. Yu, H. Li, W. He, H. Jiang, M. Li, X. Song *et al.*, “Healthgpt: A medical large vision-language model for unifying comprehension and generation via heterogeneous knowledge adaptation,” *arXiv preprint arXiv:2502.09838*, 2025.
- [36] Y. Hu, T. Li, Q. Lu, W. Shao, J. He, Y. Qiao, and P. Luo, “Omnimedvqa: A new large-scale comprehensive evaluation benchmark for medical lvlm,” in *Proceedings of the IEEE/CVF Conference on Computer Vision and Pattern Recognition*, 2024, pp. 22170–22183.
- [37] J. Choquette, “Nvidia hopper h100 gpu: Scaling performance,” *IEEE Micro*, vol. 43, no. 3, pp. 9–17, 2023.
- [38] A. Paszke, S. Gross, F. Massa, A. Lerer, J. Bradbury, G. Chanan, T. Killeen, Z. Lin, N. Gimelshein, L. Antiga *et al.*, “Pytorch: An imperative style, high-performance deep learning library,” *Advances in neural information processing systems*, vol. 32, pp. 8026–8037, 2019.
- [39] T. Dao, “Flashattention-2: Faster attention with better parallelism and work partitioning,” *arXiv preprint arXiv:2307.08691*, 2023.